
PHYSICAL PROPERTIES
OF CRYSTALS

Structural Transformations of the Dislocation Cores in Si and Their Relationship with Photoluminescence

L. I. Fedina^{a,*}, A. K. Gutakovskii^a, V. I. Vdovin^a, and T. S. Shamirzaev^a

^a Rzhanov Institute of Semiconductor Physics, Siberian Branch, Russian Academy of Sciences, Novosibirsk, 630090 Russia

*e-mail: fedina@isp.nsc.ru

Received June 9, 2020; revised August 10, 2020; accepted August 17, 2020

Abstract—As a result of in situ irradiation in a high-resolution electron microscope, structure modelling, and calculation of images, it is shown that the incorporation of self-interstitial atoms into the extension region of the core of any dislocation is accompanied by their ordering in the form of cluster-like {111}, {001}, and {113} defects, which provide core relaxation. This fact made it possible to visualize for the first time the core structure of undissociated 60° dislocations of two types, glide (60°_{sh}) and sessile (60°_{gl}), which coexist at plastic deformation of Si. It is shown that incorporation of self-interstitial atoms into the dislocation core correlates with an increase of only the *D2* line in the photoluminescence spectrum, while perfect sessile *a/2*(110) dislocations with a core, consisting of paired 5/7-link atomic rings without dangling bonds, are responsible for the rise of the *D1* line. This universal core occurs at coalescence of two 60°_{sh} dislocations during their slip in intersecting planes {111}, 60°_{sh} → 60°_{gl} transition, and transformation of a Frank dislocation into a perfect one.

DOI: 10.1134/S1063774521040064

INTRODUCTION

Although photoluminescence (PL) of dislocations in Si due to radiative recombination of electrons and holes on dislocation centers [1] have been studied for many years, it is still not completely understood because of the variety of dislocations and their transformations, which impede establishment of correlations between the dislocation structure and PL. This phenomenon was discovered in 1976 for plastically deformed Si by Drozdov et al. [2] using PL spectroscopy. Four emission bands were found in the Si PL spectrum, which are denoted according to the position of their peaks: lines *D1* (0.812 eV), *D2* (0.875 eV), *D3* (0.937), and *D4* (1.00 eV). Dislocation PL is of practical interest because of its possible application for designing Si LEDs emitting in the range of 1.5–1.6 μm (0.812 eV) [3], which can be integrated in the complementary metal-oxide semiconductor (CMOS) technology [4].

Among the four lines found in plastically deformed Si, the *D3/D4* lines are assumed to be of known origin and related to the dissociation of glide 60° dislocations [5–7]. However, the nature of the *D1/D2* lines is questionable, because their occurrence is independent of the way of dislocation introduction [1–5, 8, 9], although the structures and mechanisms of dislocation formation radically differ. For example, dislocations introduced by ion implantation and annealing are sessile; they cannot dissociate. Therefore, only the *D1/D2* lines are observed in the PL spectra [9].

At plastic deformation of Si, the structure of 60° dislocations differs, depending on slip in the shuffled set of the {111} planes (between bilayers) and glide set (inside a bilayer) [10]. The slip is performed via undissociated dislocations of the shuffled set (60°_{sh}) in the first case and by dissociated dislocations (60°_{dis}) in the second case. The slip of 60°_{sh} dislocations is related to kinetic limitations on the motion of kinks of partial Shockley dislocations and, therefore, is implemented at high temperatures [7]. It was shown in [11] that 60°_{sh} dislocations introduced into Si at room temperature are presumably optically nonactive. However, their annealing induces a PL spectrum with all *D1–D4* lines [12]. This indicates a transition of dislocations from the shuffled to glide set (60°_{sh} → 60°_{gl}) and their dissociation (60°_{gl} → 60°_{dis}). As was suggested in [13], this scenario requires emission of an atom from the 60°_{sh} core, which provides its climb to the glide set of the {111} planes. According to [13], the 60°_{sh} core should consist of an eight-link ring with one dangling bond, while the 60°_{gl} core should consist of double 5/7-link atomic rings (core 5/7). It was shown by means of in situ annealing of 60°_{sh} dislocations in an electron microscope using a weak beam that dissociation is implemented locally, mainly at curvilinear dislocation portions [14]. The major part of the dislocation line remains undissociated. Therefore, the occurrence of the *D1/D2* lines after annealing of 60°_{sh} dislocations, gliding over one system of the {111} planes [12], indi-

icates existence of 60_{gl}° dislocation portions, which avoid dissociation (due to the kinetic limitations [7, 15]) and become optically active. Ab initio calculations for a diamond lattice suggest high stability of the 60_{gl}° dislocation core due to the reconstruction of atomic bonds along the dislocation line [16].

Application of high-resolution electron microscopy (HREM) for analyzing the dislocation structure in relaxed semiconductor heterostructures reveals two types of the sessile 90° Lomer dislocation with the core structure of 5/7-link (L_{sh}) and single eight-link (L_{gl}) ring with two dangling bonds [17, 18]. This dislocation is known to arise due to the interaction of two 60° dislocations gliding in the crossed $\{111\}$ planes [19]. Therefore, the existence of Lomer dislocations of two types (L_{sh} and L_{gl}) confirms indirectly the presence of two types for the 60° dislocation (60_{sh}° and 60_{gl}°). However, the existence of the 60_{gl}° dislocation was not confirmed experimentally. Moreover, according to the ab initio calculations [20], there are four possible core configurations for the 60° dislocation: $S1$, $S2$, $S3$, and G , belonging to the shuffled (S) and glide (G) sets. Among these four configurations, only the most metastable core $S1$ (corresponding to the 60_{sh}° core proposed in [13]) is mobile in Si. The other three cores ($S2$, $S3$, and G) are sessile, and the most stable one is of the G type with the core structure corresponding to 60_{gl}° .

Taking into account this pathological variety of dislocations coexisting in a Si crystal [10], the problem of revealing the nature of $D1/D2$ lines seems to be unsolvable. In addition, ab initio calculations show yield that these lines may be related to clusters of self-interstitial atoms (I_s) in the dislocation core, which consist of three (I_3) or four (I_4) atoms [21, 22]. Clusters I_3 and I_4 correspond to a short $\langle 110 \rangle$ chain of three atoms and a flat cluster lying in the $\{001\}$ plane, respectively. Incorporation of individual, mutually unrelated $\langle 110 \rangle$ I_s chains into the stretched part of the Frank dislocation core in the $\{111\}$ plane with (2×1) ordering due to the bond reconstruction was observed for the first time in situ by the HREM method under irradiation [23]. This defect (referred to as the $\{111\}$ defect) in the (110) cross section is characterized by a sequence of double five-link and single eight-link atomic rings. It was shown that the formation of the $\{111\}$ defect in the dislocation core provides its relaxation, so that the Burgers vector decreases from $a/3\langle 111 \rangle$ to $a/8\langle 111 \rangle$. Each I_s chain in the (2×1) structure is actually visualized in an HREM [110] image as the I_3 cluster forming double five-link rings [21, 22]. To retain the valence, atoms along the I_s chain are pairwise related (as in the I_3 cluster), and their number is determined by the irradiation time [23]. The possibility of using in situ irradiation in the HREM method to solve the problem of $D1/D2$ lines was demonstrated in [24], where the relationship between the $D2$ line

with the I_s ordering in the core of 60_{sh}° dislocations was confirmed. This made it possible to visualize the structure of the 60_{sh}° core consisting of an eight-link ring with a dangling bond. However, the questions of visualization of the 60_{gl}° dislocation at plastic deformation and its possible contribution to the $D1$ line remain open.

The purpose of this study was to search for a universal dislocation core in Si, which can explain the occurrence of the $D1$ line in PL spectra, regardless of the way of dislocation introduction.

EXPERIMENTAL

Frank dislocation loops and perfect dislocations were formed using implantation of Si^+ , B^+ , and O^+ ions with energy of 30–50 keV (to a dose of 4×10^{14} and 10^{16} cm^{-2}), with subsequent annealing at $T = 900\text{--}1000^{\circ}\text{C}$. Glide dislocations in silicon grown by the floating-zone method (Fz-Si) were introduced using plastic deformation at crystal growth suppression due to a spillage of the molten zone (implementation of thermal shock). Their density was $10^6\text{--}10^8 \text{ cm}^{-2}$. HREM analysis and in situ electron irradiation were performed in a JEM4000EX microscope with an energy of 400 keV at room temperature and electron fluence of $\sim 10^{20} \text{ cm}^{-2} \text{ s}^{-1}$. The corresponding PL spectra of Fz-Si were obtained before and after irradiation of the sample surface with an area of $\sim 1 \text{ cm}^2$ by a 350-keV external electron gun to a dose of $\sim 10^{20} \text{ cm}^{-2}$. The HyperChem-8.0 commercial software and the MUSLI program [25] were used to create relaxed models and calculate the HREM images of dislocations in a cell $102 \times 102 \times 112 \text{ \AA}$ in size. PL was excited by an Ar^+ laser at a wavelength $\lambda = 488 \text{ nm}$ and recorded at a sample temperature of 4.2 K using an EI-L Ge $p\text{--}i\text{--}n$ photodiode.

Structure and Photoluminescence of Glide 60° Dislocations

Figure 1a presents a TEM image of a 60° dislocation in Fz-Si, recorded in a weak beam, which demonstrates the absence of its dissociation. An HREM image of this dislocation in the (110) cross section is given in Fig. 1b. The Burgers contour, constructed according to the image, yields a vector $\mathbf{b} = a/2\langle 110 \rangle$, lying in the $\{111\}$ plane and corresponding to a glide 60° dislocation. Its theoretical HREM image is given in the inset in Fig. 1b. The image was calculated using the model of 60_{sh}° dislocation (Fig. 2a) proposed in [13]. A comparison of the experimental and calculated HREM images shows their good consistency, which suggests adequacy of the model in use. However, the structure of the 60_{sh}° dislocation core cannot be constructed by proceeding from the HREM image; it may be different.

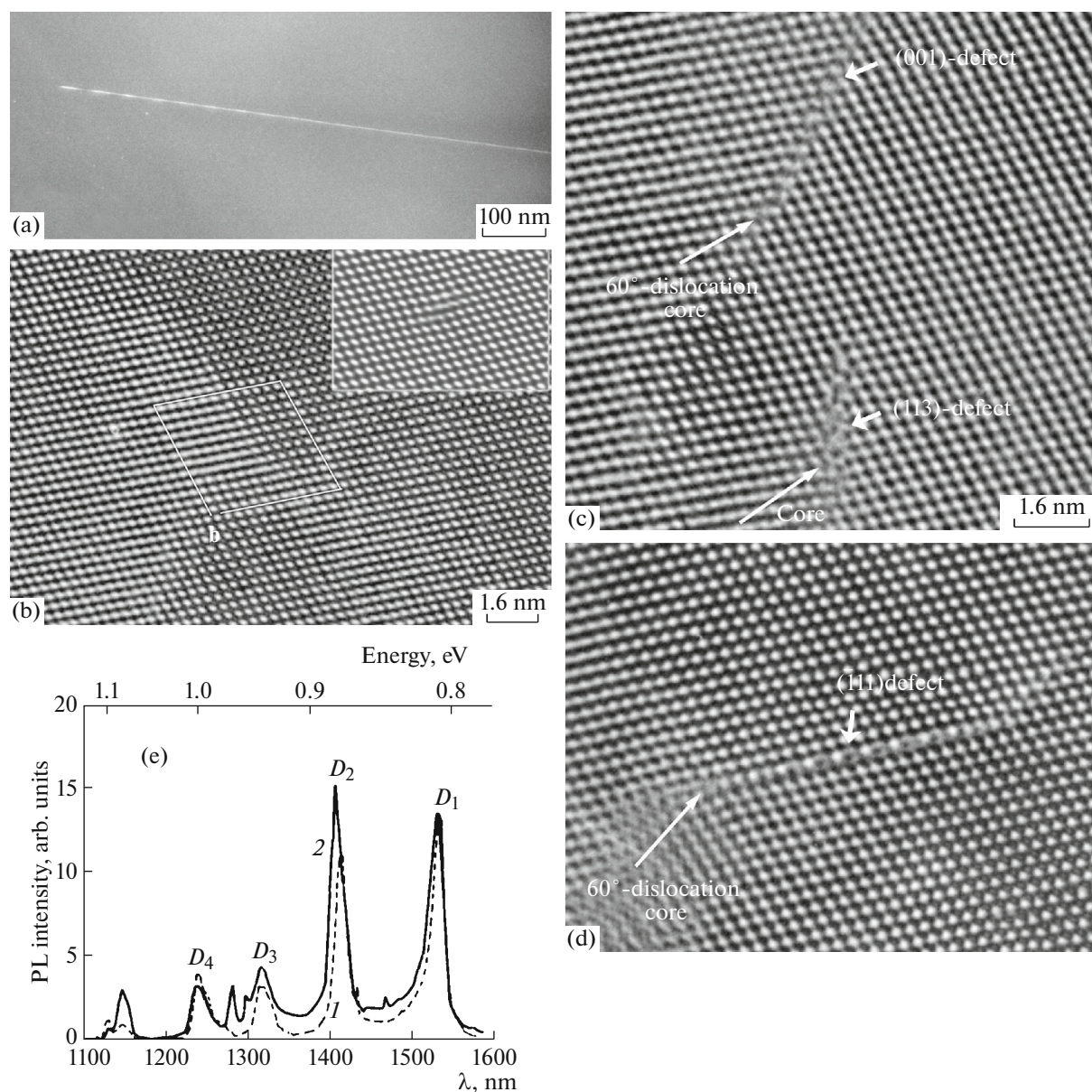


Fig. 1. (a) TEM image obtained in a weak beam and (b–d) HREM images in the (110) cross section of a 60° dislocation in Fz-Si (b) before and (c, d) after short-term (~ 1 – 2 min) in situ electron irradiation in a JEM-4000EX microscope at room temperature. The calculated HREM image of the 60°_{sh} dislocation is given in the inset (crystal thickness 9.3 nm, defocusing value -45 nm). The Burgers contour is outlined by a rhombus made of white lines (b), and arrows indicate the position of the dislocation core. (e) PL spectra of Fz-Si (1) before and (2) after electron irradiation by an external pulsed gun.

To understand if the two types of the core of undissociated 60° dislocation can be distinguished, the existing 60°_{sh} model was supplemented with the 60°_{gl} model, and their calculated HREM images were subjected to comparative analysis (Fig. 2). The HREM images were obtained at two defocusing: optimal (Scherzer) and far from optimal, at the crystal thickness of 6.2 nm, when the 60°_{sh} and 60°_{gl} core structures are directly projected on the (110) image plane (atomic columns are shown dark). It can be seen that the 60°_{sh}

and 60°_{gl} core images slightly differ only under optimal conditions (Figs. 2b, 2e). These differences disappear far from the Scherzer defocusing because of the image inversion (Figs. 2c, 2f). This means that the 60°_{sh} and 60°_{gl} dislocations are fairly difficult to be distinguished experimentally.

Other possibilities for analyzing the structure of the 60°_{sh} and 60°_{gl} dislocation cores are provided when using in situ HREM irradiation (Figs. 1c, 1d). In this case, HREM images demonstrate the formation of all

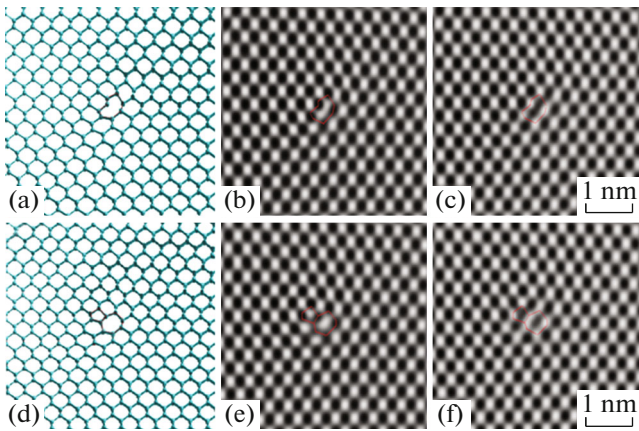


Fig. 2. Structural models and calculated HREM images in the (110) cross section of (a–c) 60_{sh}° and (d–f) 60_{gl}° dislocations. The calculation parameters are as follows: sample thickness 6.2 nm, accelerating voltage 400 kV, spherical aberration coefficient 1 mm, defocusing (b, e) -36 and (c, f) -103 nm. Lines show the configurations of the 60_{sh}° and 60_{gl}° cores.

known ordered I_s structures in the $\{111\}$, $\{001\}$, and $\{113\}$ planes [23, 26, 27] in the stretched part of the core of the observed 60° dislocations. It is known that these defects arise also in Si in the absence of dislocations under irradiation with electrons and light ions up to $T \approx 700^{\circ}\text{C}$ [26]. Obviously, the strain field of the dislocation core serves as the nucleation center of metastable I_s forms. Because of the presence of kinetic limitations on the incorporation of interstitial atoms into nodal sites in the extra-plane of interstitials ending in the core [28], I_s can be accumulated only near the core dislocations at $T \sim 20^{\circ}\text{C}$. The existence of two types of metastable defects, $\{111\}$ and $\{001\}$, indicates the presence of these half-planes in the 60° dislocation core. The formation of $\{113\}$ defects has a more complex character, related to the joint clusterization of vacancies and interstitial atoms [29–31]. After by irradiation by an external electron gun, the PL spectra exhibit an increase of only the $D2$ line, whereas the $D1$ line intensity does not change (Fig. 1e, solid line 2). This behavior confirms the direct relationship between the occurrence of ordered clusters of intrinsic interstitial atoms in the dislocation core and the enhancement of the $D2$ line.

Incorporation of I_s into the core provides not only its relaxation but also visualization (allows one to construct the core structure based on the HREM image). Figure 3 shows experimental and calculated HREM images of the (001) defect occurring near the 60° dislocation core, along with its model constructed based on the experimental image. Although the (001) defect structure does not attain equilibrium state in the experiment for the short irradiation time (in contrast to the relaxed model used to calculate the image), the

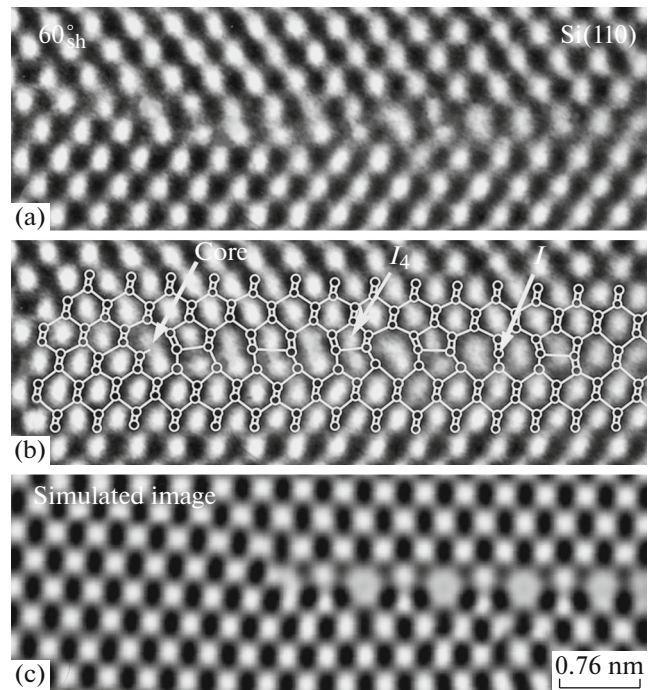


Fig. 3. (a, b) Experimental and (c) calculated HREM images of the (001) defect attached to the 60_{sh}° core, along with the model constructed based on the image in panel b. The calculation parameters are as follows: defocusing 40 nm, crystal thickness 6.2 nm. Arrows from left to right indicate, respectively, the 60_{sh}° core, perfect I_4 cluster, and reconstruction defect in the (001) defect plane.

experimental image is in good agreement with the calculated one. One can clearly see in Fig. 3b that the 60° dislocation core consists of an eight-link ring, corresponding to the 60_{sh}° dislocation core. Multiple flat I_4 clusters lying in the (001) plane are ordered near the core and form a (2×1) superstructure. Each I_4 cluster in the HREM image is presented by a pair of atoms related to the matrix by double five-link rings. Bonds between the atomic pairs in neighboring layers in the HREM image [110] are not shown. This cluster configuration is completely consistent with the ab initio calculations [21, 22]. Molecular dynamics calculations show that $\{001\}$ defects may occur both at crystal extension and in the absence of deformations [32].

Similar (2×1) ordering of interstitial atoms can be seen in Fig. 4 for the $\{111\}$ defect attached to the core of another 60° dislocation, with the only difference: in this case, interstitial atoms form $\langle 110 \rangle$ chains (similar to the atomic chain in the I_3 cluster [21, 22]). Along a long continuous chain, atomic pairs are interrelated, forming four-atom clusters, which are not seen in the HREM image. The Burgers contour, constructed based on the HREM image of the dislocation, shows that dislocation is a glide one (Fig. 4b), because its Burgers vector lies in the $\{111\}$ plane. However, the model constructed using the image exhibits the

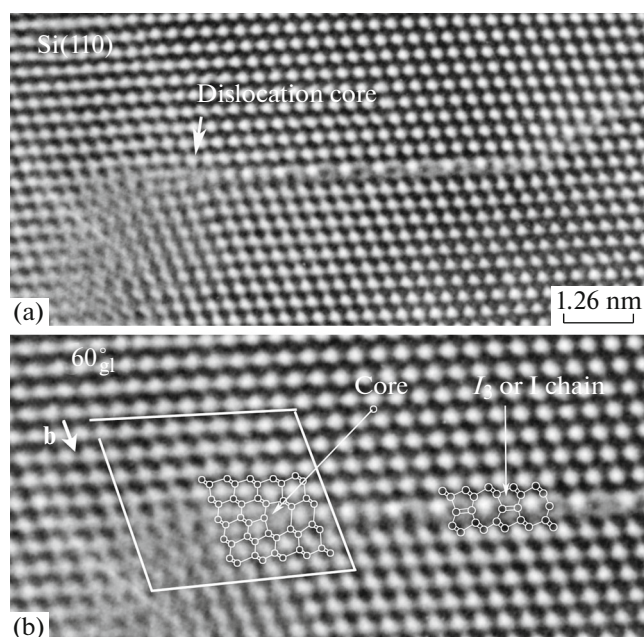


Fig. 4. (a) Experimental HREM images of the 60°_{gl} dislocation with the $\{111\}$ defect attached to its core and (b) model constructed using the image. The Burgers contour of the dislocation and positions of I_3 chains (I_3 clusters) in the $\{111\}$ defect plane are indicated by a diamond and an arrow, respectively.

$5/7$ core, which corresponds to the 60°_{gl} dislocation [16]. This fact confirms that the attachment of interstitial atoms to the dislocation core facilitates its relaxation and HREM visualization. The fact that the 60°_{sh} and 60°_{gl} dislocations coexist in plastically deformed Si suggests that the $D1$ line can be assigned to both the 90° Lomer dislocation L_{sh} , occurring at coalescence of 60°_{sh} dislocations during their slip, and the 60°_{gl} dislocation, because they both are characterized by the $5/7$ core with bond reconstruction in the 60°_{gl} core along the dislocation.

Structure and Photoluminescence of Dislocations in Ion-Implanted Si

The formation and growth of Frank dislocation loops of the interstitial type in Si under ion implantation have been thoroughly investigated [26]. These loops are high-temperature forms of interstitial atomic clusters in the $\{111\}$ plane, the structure of which corresponds to 90° sessile dislocations with the Burgers vector $a/3\langle 111 \rangle$ (90°_{fr}). Incorporation of interstitial atoms in the twin configuration provides occurrence of a stacking fault in the 90°_{fr} loop plane. Having reached a certain size, the 90°_{fr} loop loses stability and is transformed into a perfect prismatic loop with the Burgers vector $a/2\langle 110 \rangle$ [33]. This process is known to be related to the slip of two Shockley dislocations in

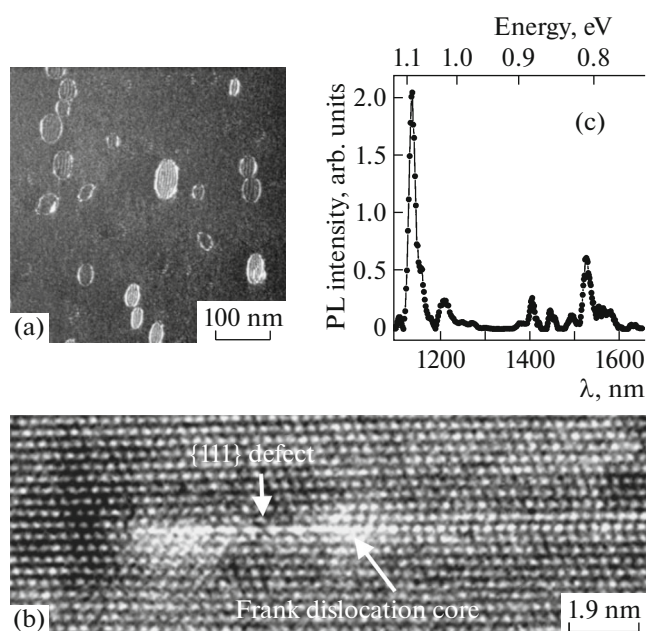


Fig. 5. (a) TEM image and (b) HREM image in the (110) cross section of Frank dislocations introduced into Si using implantation with Si^+ ions and annealing at $1000^\circ C$. (c) PL spectrum of the sample ($T = 5$ K).

the loop plane [34]. However, the structure of the perfect dislocations occurring during implantation has never been studied. An increase in their fraction in implanted Si is accompanied by an increase in the $D1$ line intensity [9].

Figures 5a and 5b show, respectively, the dark-field TEM and HREM images of the Frank loops in Si, introduced by implantation of Si^+ ions (to a dose of $4 \times 10^{14} \text{ cm}^{-2}$) and annealing at $T = 1000^\circ C$. As can be seen in the HREM image, a $\{111\}$ defect, similar to that near the 60°_{gl} core (Fig. 1d), occurs immediately near the 90°_{fr} core. The PL spectrum of the sample (Fig. 5c) demonstrates weak optical activity of 90°_{fr} dislocations.

In Si implanted with B^+ and O^+ ions (to a dose of $1 \times 10^{16} \text{ cm}^{-2}$), after annealing at $T = 900\text{--}1000^\circ C$, one can see a mixture of 90°_{fr} loops and perfect loops, as well as long dislocation dipoles (Figs. 6a, 6b). These dipoles are the result of the transformation of $\{113\}$ defects after exceeding their stability temperature $T \sim 700^\circ C$ [26]. The HREM image of the 90°_{fr} dislocation in Si, introduced by implantation of O^+ ions and annealing at $1000^\circ C$ (Fig. 6c), exhibits a small $\{111\}$ defect near its core. This image was obtained in a JEM-2010FX microscope at an accelerating voltage of 200 kV, which excludes generation of point defects in the microscope at room temperature [35]. This means that the $\{111\}$ defect was formed during annealing of implanted Si. Among various metastable forms of I_3 , the $\{111\}$ defect is most stable; its energy does not

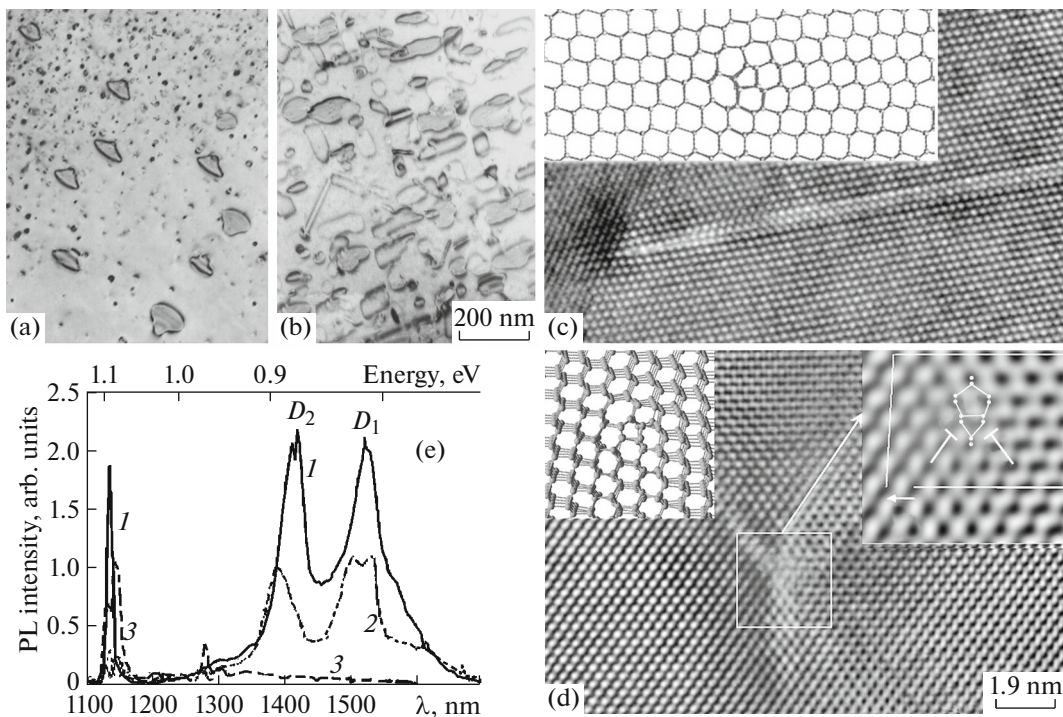


Fig. 6. (a, b) TEM images in the (001) cross section and (c, d) HREM images in the (110) cross section of (c) Frank and (d) perfect dislocations introduced by implantation of B^+ and O^+ ions at (a) 900 and (b–d) 1000°C. Results of computer simulation of the 90°_{fr} dislocation and perfect dislocation are given in the corresponding insets. The inset on the right of panel (d) shows an enlarged HREM image of the perfect dislocation core. (e) PL spectra in Si implanted with (1, 2) O^+ and (3) B^+ ions (to a dose of 10^{16} cm^{-2}) after annealing at (2, 3) 900 and (1) 1000°C; $T = 4.2 \text{ K}$.

exceed $\sim 0.3 \text{ eV/atom}$ [23], whereas the energy of the $\{113\}$ defect is $\sim 1 \text{ eV/atom}$ [26]. Therefore, $\{111\}$ defects in ion-implanted Si should make the main contribution to the $D2$ line (Fig. 6e).

TEM and PL analyses show that the transformation of 90°_{fr} loops into the perfect ones is accompanied by an increase in the $D1$ line strength (Fig. 6e). It follows from a comparison of Figs. 6e and 5c that the intensity of the $D1$ line, corresponding to the mixture of perfect loops and dipoles, is higher by a factor of 40 than the strength of the line due to 90°_{fr} loops in Si implanted with Si^+ ions. Moreover, in the case of implantation with B^+ and annealing at $T = 900^\circ\text{C}$ (when solely 90°_{fr} loops are observed in Si (Fig. 6a)), PL is completely absent (Fig. 6e, curve 3). This fact indicates that 90°_{fr} dislocations are optically nonactive.

Figure 6d shows an HREM image of a perfect dislocation in Si, which is characterized by the presence of strong deformations around the core. Two $\{111\}$ extraplanes ending in the core can be seen in an enlarged HREM image of the core region (Fig. 6d, inset on the right); at closed bonds, these extraplanes form the $5/7$ core corresponding to the structure of the 90° Lomer dislocation L_{sh} . The Burgers contour, constructed around the dislocation, confirms that its

Burgers vector \mathbf{b} does not lie in the $\{111\}$ plane and corresponds to L_{sh} .

The model of perfect dislocation occurring after the transformation of the 90°_{fr} dislocation is presented in the inset in Fig. 6d. This process was simulated using the HyperChem-8.0 program. Realization of slip of two partial Shockley dislocations in the plane of the 90°_{fr} loop (Fig. 6c) above and below the incorporated layer of interstitial atoms in the twin configuration leads indeed to the formation of the $5/7$ core corresponding to the L_{sh} structure. The model core also exhibits significant deformations, which do not make it possible to give a clear plane projection.

A comparison of the 90°_{fr} and L_{sh} models (Figs. 6c and 6d, insets) shows that both cores consist of $5/7$ -unit atomic rings; however, only L_{sh} yields the $D1$ line in the PL spectra (Fig. 6e). The main difference between these models is that two identical “diamond” $\{111\}$ extraplanes end in the L_{sh} core, whereas in the 90°_{fr} core one of them is a stacking fault. The presence of a stacking fault in the 90°_{fr} dislocation core, as was shown by multiscale ab initio calculations [36], leads to disappearance of its optical activity due to the displacement of dislocation level to the edge of the conduction band in Si. For the L_{sh} dislocation, a level of $\sim 0.2 \text{ eV}$ arises in the band gap of Si.

The splitting of the *D1* line between 0.812 and 0.830 eV, observed in the PL spectrum (Fig. 6e, curve 2), is related to the formation of oxide precipitates with a high density ($\sim 10^{11} \text{ cm}^{-2}$) in Si implanted with O^+ ions to a high dose. A similar PL feature caused by oxygen precipitates was observed in [37].

Thus, based on a detailed analysis of the structure of dislocations in ion-implanted Si and their PL, it was unambiguously established that perfect dislocations having a structure of the L_{sh} (5/7) core without dangling bonds are responsible for the enhancement of the *D1* line.

CONCLUSIONS

The performed investigations confirmed the existence of a 60_{gl}° dislocation with a 5/7 core structure in plastically deformed Si. This finding makes it possible to formulate the concept of universal configuration of the dislocation core in the form of paired 5/7-unit atomic rings without dangling bonds to explain the enhancement of the *D1* line in the PL spectrum, regardless of the way of dislocation introduction. This core occurs at coalescence of two 60_{sh}° dislocations in the case of their slip, $60_{\text{sh}}^{\circ} \rightarrow 60_{\text{gl}}^{\circ}$ transition, and transformation of the Frank dislocation into a perfect one. The fact that ordering of interstitial atoms is observed near the core of any dislocation, irrespective of its optical activity, indicates the absence of correlation between the *D1* and *D2* lines.

ACKNOWLEDGMENTS

This study was performed using equipment of the CKP Nanostruktury of the Rzhanov Institute of Semiconductor Physics.

FUNDING

This study was supported by the Russian Science Foundation (project no. 19-72-30023).

REFERENCES

- V. Kveder and M. Kittler, *Mater. Sci. Forum* **590**, 29 (2008). doi 10.4028/www.scientific.net/MSF.590.29
- N. A. Drozdov, A. A. Patrin, and V. D. Tkachev, *JETP Lett.* **23**, 597 (1976).
- V. Kveder, M. Badylevich, E. Steinman, et al., *Appl. Phys. Lett.* **84**, 2106 (2004). <https://doi.org/10.1063/1.1689402>
- M. Reiche and M. Kittler, *Crystals* **6**, 74 (2016). <https://doi.org/10.3390/cryst6070074>
- R. Sauer, J. Weber, J. Stolz, et al., *Appl. Phys. A* **36**, 1 (1985). <https://doi.org/10.1007/BF00616453>
- K. Wessel and H. Alexander, *Philos. Mag.* **35**, 1523 (1977). <https://doi.org/10.1080/14786437708232975>
- H. R. Kolar, J. Spence, and H. Alexander, *Phys. Rev. Lett.* **77**, 4031 (1996). <https://doi.org/10.1103/PhysRevLett.77.4031>
- E. A. Steinman, V. I. Vdovin, T. G. Yugova, et al., *Semicond. Sci. Technol.* **14**, 582 (1999).
- N. A. Sobolev, O. B. Gusev, E. I. Shek, et al., *Appl. Phys. Lett.* **72**, 3326 (1998). <https://doi.org/10.1063/1.121593>
- J. Rabier, *Philos. Mag. A* **93**, 162 (2013). <https://doi.org/10.1080/14786435.2012.691217>
- S. Pizzini, S. Binetti, A. Le Donne, et al., *Appl. Phys. Lett.* **88**, 211910. DOI (2006). <https://doi.org/10.1063/1.2206874>
- A. N. Tereshchenko, E. A. Steinman, and J. Rabier, *J. Phys.: Conf. Ser.* **281**, 012020 (2011). <https://doi.org/10.1088/1742-6596/281/1/012020>
- J. Hornstra, *J. Phys. Chem. Solids* **5**, 129 (1958).
- H. Saka, K. Yamamoto, S. Arai, et al., *Philos. Mag.* **86**, 4841 (2006). <https://doi.org/10.1080/14786430600764898>
- Z. Li and R. C. Picu, *J. Appl. Phys.* **113**, 083519 (2013). <https://doi.org/10.1063/1.4793635>
- A. T. Blumenau, M. I. Heggie, C. J. Fall, et al., *Phys. Rev. B* **65**, 205205 (2002). <https://doi.org/10.1103/PhysRevB.65.205205>
- Y. Wang, P. Ruterana, S. Kret, et al., *J. Appl. Phys.* **100**, 262110 (2012). <https://doi.org/10.1063/1.4731787>
- C. Wen, *Microsc. Microanal.* **23**, 449 (2017). <https://doi.org/10.1017/S1431927617000137>
- W. M. Lomer, *Philos. Mag.* **42**, 334 (1951).
- L. Pizzagalli, J. Godet, and S. Brochard, *Phys. Rev. Lett.* **103**, 065505 (2009). <https://doi.org/10.1103/PhysRevLett.103.065505>
- R. Jones, B. J. Coomer, J. P. Goss, et al., *Phys. Status Solidi B* **222**, 133 (2000). [https://doi.org/10.1002/1521-3951\(200011\)222:1<133::AID-PSSB133>3.0.CO;2-D](https://doi.org/10.1002/1521-3951(200011)222:1<133::AID-PSSB133>3.0.CO;2-D)
- A. T. Blumenau, R. Jones, S. Öberg, et al., *Phys. Rev. Lett.* **87**, 187404 (2001). <https://doi.org/10.1103/PhysRevLett.87.187404>
- L. Fedina, A. Gutakovskii, A. Aseev, et al., *Philos. Mag. A* **77**, 423 (1998). <https://doi.org/10.1080/01418619808223762>
- L. I. Fedina, A. K. Gutakovskii, and T. S. Shamirzaev, *J. Appl. Phys.* **124**, 053106 (2018). <https://doi.org/10.1063/1.5011329>
- A. Chuvilin and U. Kaizer, **104**, 73 (2005). <https://doi.org/10.1016/j.ultramic.2005.03.003>
- A. Aseev, L. Fedina, D. Hoehl, et al., *Clusters of Interstitial Atoms in Silicon and Germanium* (Academy Verlag, Berlin, 1994).
- S. Takeda, M. Kahyama, and K. Ibe, *Philos. Mag. A* **70**, 287 (1994). <https://doi.org/10.1080/01418619408243186>
- L. I. Fedina and A. L. Aseev, *Phys. Status Solidi A* **95**, 517 (1986). <https://doi.org/10.1002/pssa.2210950220>
- L. I. Fedina, A. K. Gutakovskii, A. V. Latyshev, et al., *Advances in Semiconductor Nanostructures* (Elsevier, 2017), Ch. 16.

30. L. I. Fedina, Ahn Song Se, A. L. Chuvilin, et al., *Microsc. Microanal.* **19** (5), 32 (2013).
<https://doi.org/10.1017/S1431927613012294>
31. N. A. Sobolev, A. E. Kalyadin, E. I. Shek, et al., *Phys. Status Solidi A* **214** (7), 1700317 (2017).
<https://doi.org/10.1002/pssa.201700317>
32. S. S. Kapur and T. Sinno, *Phys. Rev. B* **82**, 045205 (2010).
<https://doi.org/10.1103/PhysRevB.82.045205>
33. L. V. Litvin, L. I. Fedina, and A. L. Aseev, *Phys. Chem. Mech. Surf.* **6**, 100 (1989).
34. J. P. Hirt and J. Lothe, *Theory of Dislocations* (New York, Wiley, 1982).
35. L. Fedina, A. L. Aseev, S. G. Denisenko, and L. S. Smirnov, *Mater. Sci. Forum.* **10–12**, 1123 (1986).
<https://doi.org/10.4028/www.scientific.net/MSF.10-12.1123>
36. W. Xie, J. Bang, and S. B. Zhang, *Mater. Res. Lett.* **2** (1), 51 (2014).
<https://doi.org/10.1080/21663831.2013.859639>
37. S. Binetti, S. Pizzini, E. Leoni, et al., *J. Appl. Phys.* **92**, 1 (2002).
<https://doi.org/10.1063/1.1497450>

Translated by A. Sin'kov